SUPPORTING INFORMATION

Unraveling the H_2 promotional effect on the Palladium catalysed CO oxidation using a combination of temporally and spatially resolved investigations

Caomhán Stewart,[†] Emma K. Gibson, [‡,∞,*] Kevin Morgan,[†,*] Giannantonio Cibin,[₸] Andrew J. Dent,[₸] Christopher Hardacre,[§] Evgenii V. Kondratenko,[¥] Vita A. Kondratenko,[¥] Colin McManus,[†] Scott Rogers,[∞, #] Cristina E. Stere,[§] Sarayute Chansai,[§] Yi-Chi Wang, [χ] Sarah J. Haigh, [χ] Peter P. Wells,[∞,₸,°] Alexandre Goguet[†]

† School of Chemistry and Chemical Engineering, Queen's University Belfast, Stranmillis Road, Belfast, BT9 5AG, UK

‡ School of Chemistry, Joseph Black Building, University of Glasgow, Glasgow, G12 8QQ, UK

∞ UK Catalysis Hub, Research Complex at Harwell, Oxfordshire, OX11 0FA, UK

₸ Diamond Light Source Ltd, Harwell Science & Innovation Campus, Didcot, Oxfordshire, OX11 0DE, UK

§ School of Chemical Engineering and Analytical Science, University of Manchester, Manchester, M13 9PL, UK

¥ Leibniz-Institut für Katalyse e.V, Universität Rostock, Albert-Einstein-Straße 29a, Rostock, D-18059, Germany

Department of Chemistry, University College London, 20 Gordon Street, London WC1H 0AJ, UK

χ School of Materials, University of Manchester, Manchester, M13 9PL

° School of Chemistry, University of Southampton, Southampton, SO17 1BJ, UK

***Corresponding authors:** emma.gibson@glasgow.ac.uk; kmorgan08@qub.ac.uk

XRD

The powder X-Ray diffraction (PXRD) measurement was carried out using a PANalytical X'Pert Pro X-ray diffractometer. The X-ray source used was copper Kα with a wavelength of 1.5405 Å. Diffractograms were collected from 15° to 90° with a step size of 0.02°. In situ diffractograms were obtained using the same experimental conditions used for the SPACI-FB-XAFS experiments.

There were no observable changes in the diffractograms over the course of the in situ experiments and a representative X-ray diffraction pattern is shown below in Figure S1, which has reflections associated with γ-Al_2O_3 (37.7, 39.9, 45.9, 61.2 and 66.9°).[1,2] No reflections characteristic of PdO (33.5, 33.8 or 54.7°)[2] or metallic Pd (40.2, 46.8 or 68.3)[2] are observed. Assuming a detection limit of 3 nm, we assume our Pd catalyst has particles smaller than this.

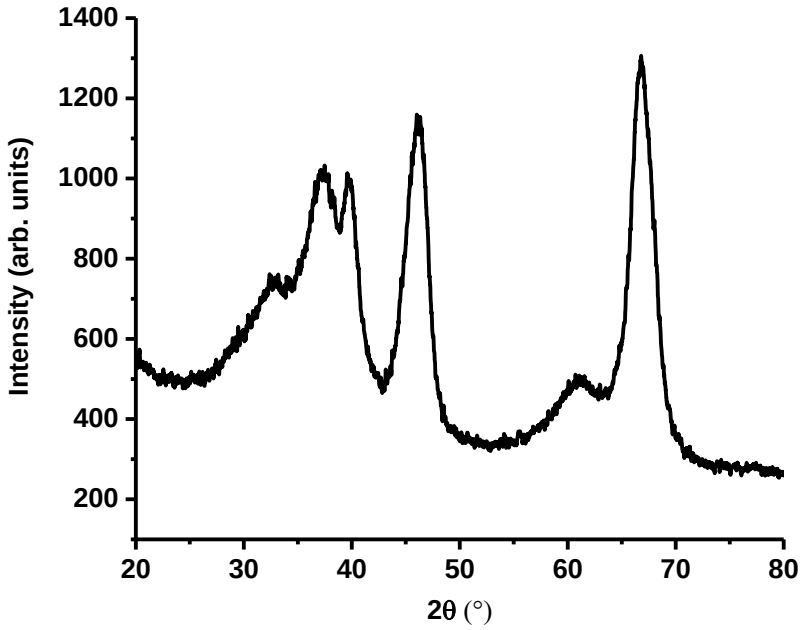

Figure S1 X-ray Diffractogram of the Pd/Al_2O_3 catalyst.

STEM

As no Pd could be detected via XRD, High-angle annular dark-field (HAADF) scanning transmission electron microscopy (STEM) was performed on the fresh catalyst. STEM HAADF images were obtained using a FEI Titan G2 80-200 (S)TEM ChemiSTEM^{TM} equipped with an X-FEG high brightness source and STEM probe aberration correction, operating at 200 keV, beam current 180 pA, 21 mrad convergence angle and a 55 mrad HAADF acceptance inner angle.

The intensity of the STEM HAADF image is proportional to the local thickness and atomic number of specimen. Pd nanoparticles are therefore observable as small regions of higher intensity on the lower intensity Al_2O_3 support. The blue circles in Figure S2 highlight some small Pd particles with diameters of between 1.0 and 1.5 nm (Figure S3).

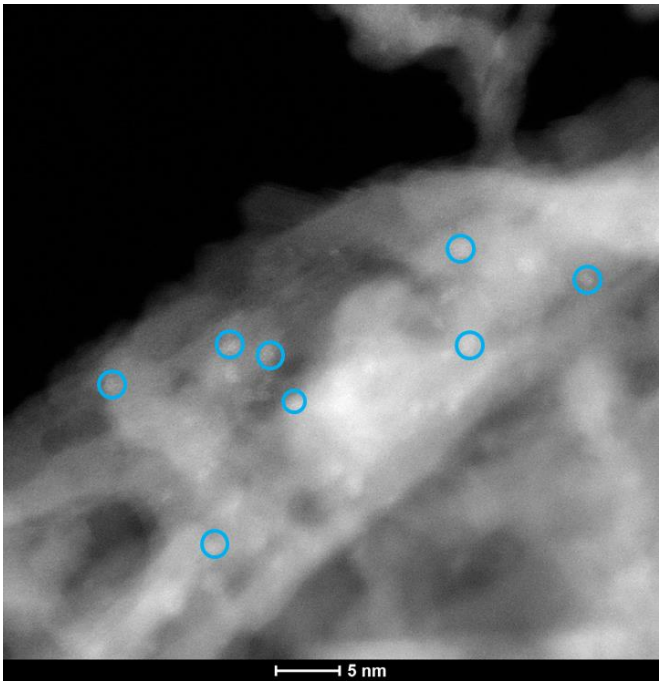

Figure S2 STEM HAADF image of Pd/Al_2O_3 catalyst.

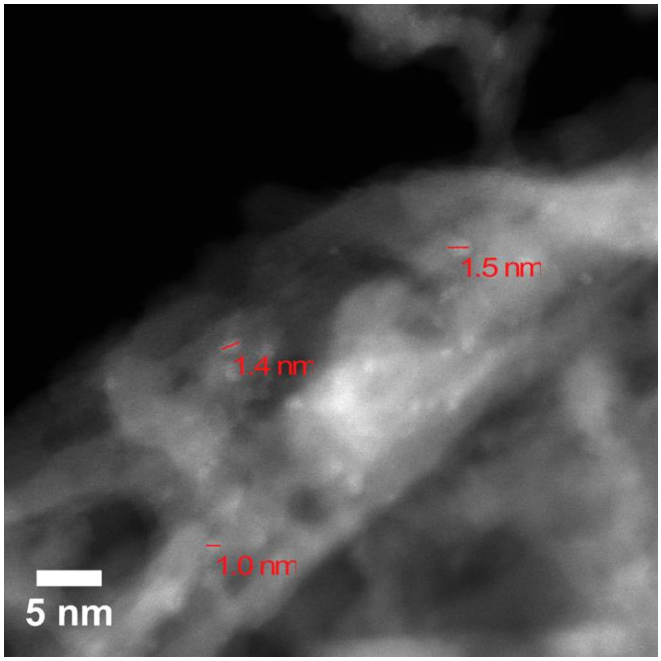

Figure S3 STEM HAADF image of Pd/Al_2O_3 catalyst showing the approximate particle diameter.

XAFS

XAFS experimental

XAFS measurements were performed at the Pd K-edge on the B18 beamline at the Diamond Light Source, Didcot, UK. Measurements were performed in transmission mode using a QEXAFS setup with fast scanning Si (311) crystal monochromator. The time resolution of the spectra was ~3.5 min/spectrum (k_{max}= 16 $Å^{-1}$). All XAFS spectra were acquired concurrently with the appropriate foil placed between I_t and I_{ref}. Spectra were collected over 15 min every 1 mm of the reactor bed to obtain sufficient signal to noise and spatial resolution.

The EXAFS analysis fitting parameters for the fresh sample in He at 100 °C, and under CO oxidation with and without H_2 are collated in Tables S1-S3. Example fits of the data are shown at the middle point of each bed in Figures S4, S5 and S6.

Table S1 Fitting parameters for the fresh catalyst after heating in helium at 100 °C. Fitting parameters: S_0^2 determined from Pd foil = 0.85, 1 < R < 3.5 Å, k-range 2.9 – 12.5, no. of independent points 15.

Conditions	**Abs-Scatterer**	**E_0 (eV)**	**CN**	**R (Å)**	**σ^2**	**R_{factor}**
He 100 Front (FIT 3)	Pd-O	0±1	3.7±0.3	2.015±0.007	0.0020±0.0008	0.01
	Pd-Pd		2.1±0.7	3.05±0.01	0.006±0.002	
	Pd-Pd		3.8±0.5	3.44±0.01	0.007	
He 100 Middle (FIT4)	Pd-O	0±1	3.7±0.3	2.014±0.008	0.002±0.0009	0.01
	Pd-Pd		2.0±0.8	3.05±0.01	0.005±0.002	
	Pd-Pd		3.6±0.6	3.44±0.01	0.007	
He 100 End (FIT 5)	Pd-O	0±2	3.8±0.4	2.02±0.01	0.003±0.001	0.02
	Pd-Pd		2±1	3.05±0.02	0.007±0.003	
	Pd-Pd		3.5±0.7	3.42±0.02	0.007	

Table S2 Fitting parameters for the catalyst under CO oxidation conditions. S_0^2 determined from Pd foil = 0.85, 1 < R < 3 Å, k-range 2.9 – 12.5, no. of independent points 11.9.

Conditions	Abs-Scatterer	E_0 (eV)	CN	R (Å)	σ^2	R_{factor}
Pos 0 (Fit 4)	Pd-O	-6.9 ± 0.6	0.6±0.2	1.97±0.03	0.0028	0.014
	Pd-Pd		7.5±0.3	2.739±0.005	0.0074	
Pos 1 (Fit 5)	Pd-O	-6.6±0.4	0.7±0.2	1.98±0.02	0.0028	0.006
	Pd-Pd		7.7±0.2	2.741±0.003	0.0074	
Pos 2 (Fit 6)	Pd-O	-6.7±0.6	0.7±0.2	1.97±0.2	0.0028	0.011
	Pd-Pd		7.5±0.3	2.740±0.004	0.0074	
Pos 3 (Fit 7)	Pd-O	-6.8±0.5	0.7±0.2	1.98±0.02	0.0028	0.01
	Pd-Pd		7.4±0.3	2.738±0.004	0.0074	
Pos 4 (Fit 8)	Pd-O	-6.9±0.6	0.6±0.2	1.97±0.03	0.0028	0.014
	Pd-Pd		7.5±0.3	2.739±0.004	0.0074	
Pos 5 (Fit 9)	Pd-O	-6.8±0.7	0.6±0.2	1.96±0.03	0.0028	0.017
	Pd-Pd		7.4±0.4	2.739±0.005	0.0074	
Pos 6 (Fit 10)	Pd-O	6.9±0.7	0.8±0.2	1.97±0.02	0.0028	0.015
	Pd-Pd		7.0±0.3	2.737±0.005	0.0074	
Pos 7 (Fit 11)	Pd-O	-6.2±0.8	1.1±0.2	1.98±0.2	0.0028	0.024
	Pd-Pd		3.0±0.4	2.740±0.006	0.0074	
Pos 8 (Fit 12)	Pd-O	-6.0±0.9	1.4±0.2	1.98±0.02	0.0028	0.026
	Pd-Pd		5.5±0.4	2.737±0.007	0.0074	
Pos 9 (Fit 13)	Pd-O	-6.1±0.8	1.4±0.2	1.98±0.01	0.0028	0.026
	Pd-Pd		5.3±0.3	2.736±0.007	0.0074	
Pos 10 (Fit 14)	Pd-O	-6.0±0.8	1.5±0.2	1.98±0.01	0.0028	0.023
	Pd-Pd		5.1±0.3	2.727±0.006	0.0074	
Pos 11 (Fit 15)	Pd-O	-5.6±0.8	1.7±0.2	1.98±0.01	0.0028	0.018
	Pd-Pd		4.7±0.3	2.741±0.006	0.0074	
Pos 12 (fit 16)	Pd-O	-5.4±0.9	1.9±0.2	1.98±0.01	0.0028	0.020
	Pd-Pd		4.7±0.3	2.745±0.007	0.0074	

Table S3 Fitting parameters for the catalyst under PROX oxidation conditions. S_0^2 determined from Pd foil = 0.85, 1 < R < 3 Å, k-range 2.9 – 11.9, no. of independent points 11.2.

Conditions	**Abs-Scatterer**	**E_0 (eV)**	**CN**	**R (Å)**	**σ^2**	**R_{factor}**
Pos 0 (Fit 4)	Pd-O	-5.1±0.6	0.6±0.2	1.97±0.03	0.0028	0.011
	Pd-Pd		7.5±0.3	2.74±0.005	0.0074	
Pos 1 (Fit 5)	Pd-O	-4.7±0.9	1.2±0.2	1.97±0.02	0.0028	0.022
	Pd-Pd		5.7±0.4	2.733±0.007	0.0074	
Pos 2 (Fit 6)	Pd-O	-4±1	1.3±0.3	1.97±0.02	0.0028	0.034
	Pd-Pd		5.4±0.4	2.734±0.008	0.0074	
Pos 3 (Fit 7)	Pd-O	-4.5±0.9	1.3±0.2	1.98±0.02	0.0028	0.024
	Pd-Pd		5.4±0.4	2.736±0.007	0.0074	
Pos 4 (Fit 8)	Pd-O	-4.5±0.9	1.4±0.2	1.97±0.02	0.0028	0.025
	Pd-Pd		5.4±0.4	2.736±0.007	0.0074	
Pos 5 (Fit 9)	Pd-O	-4.7±0.9	1.3±0.2	1.98±0.02	0.0028	0.022
	Pd-Pd		5.4±0.4	2.734±0.007	0.0074	
Pos 6 (Fit 10)	Pd-O	-5±1	1.4±0.2	1.98±0.02	0.0028	0.027
	Pd-Pd		5.4±0.4	2.735±0.007	0.0074	
Pos 7 (Fit 11)	Pd-O	-5±1	1.4±0.2	1.97±0.02	0.0028	0.028
	Pd-Pd		5.3±0.4	2.734±0.008	0.0074	
Pos 8 (Fit 12)	Pd-O	-4.2±0.8	1.6±0.2	1.98±0.01	0.0028	0.016
	Pd-Pd		5.4±0.3	2.738±0.006	0.0074	
Pos 9 (Fit 13)	Pd-O	-4±1	1.7±0.2	1.98±0.01	0.0028	0.026
	Pd-Pd		5.1±0.4	2.738±0.008	0.0074	
Pos 10 (Fit 14)	Pd-O	-4±1	1.7±0.2	1.98±0.01	0.0028	0.027
	Pd-Pd		4.8±0.4	2.739±0.008	0.0074	
Pos 11 (Fit 15)	Pd-O	-4±1	1.8±0.2	1.98±0.01	0.0028	0.028
	Pd-Pd		4.7±0.4	2.742±0.008	0.0074	
Pos 12 (fit 16)	Pd-O	-3.9±0.9	1.9±0.2	1.99±0.01	0.0028	0.018
	Pd-Pd		4.7±0.3	2.741±0.007	0.0074	

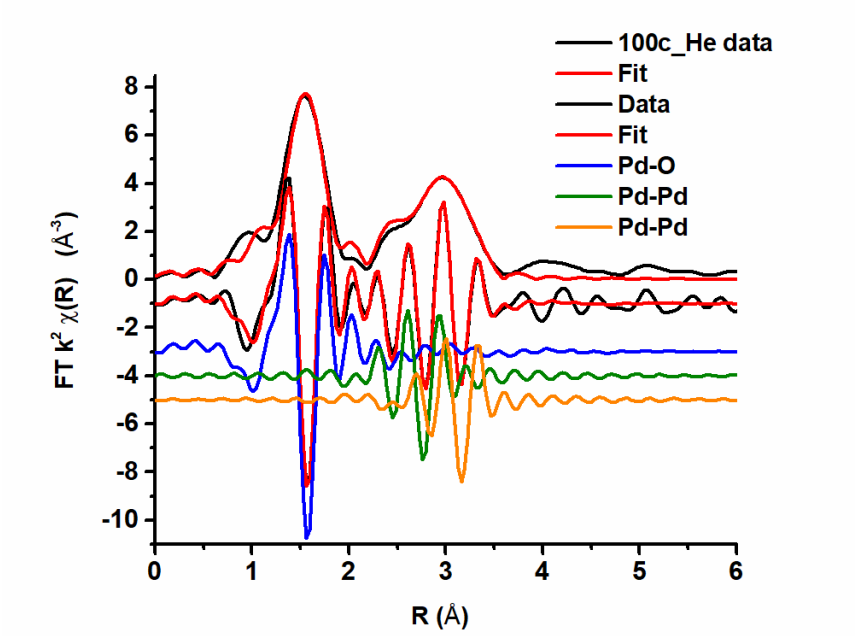

Figure S4 Magnitude component and imaginary parts of the scattering paths of the k^3 Fourier Transform of the EXAFS data for the middle of the bed under helium at 100 °C.

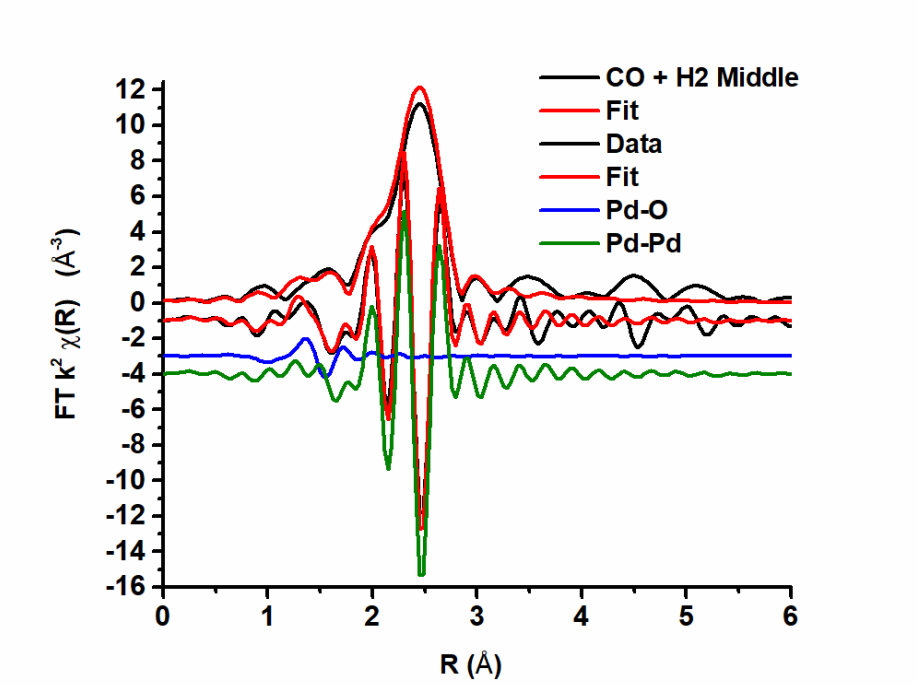

Figure S5 Magnitude component and imaginary parts of the scattering paths of the k^3 Fourier Transform of the EXAFS data for the middle of the bed under CO oxidation conditions.

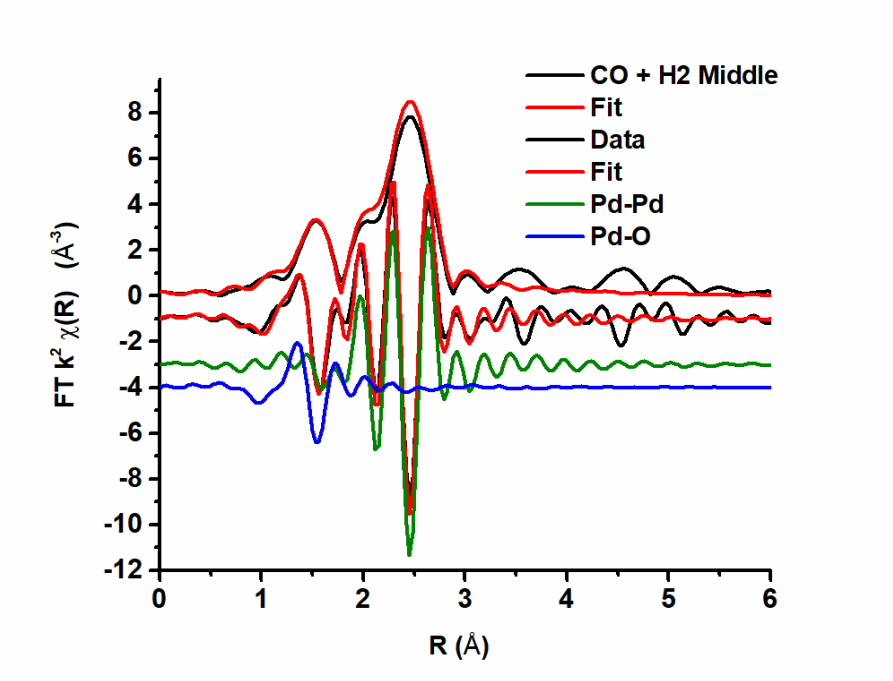

Figure S6 Magnitude component and imaginary parts of the scattering paths of the k^3 Fourier Transform of the EXAFS data for the middle of the bed under CO oxidation with H_2 conditions.

Tables S4 and S5 collate the linear combination data as shown in Figure 3, using the spectra of a PdO reference and the Pd foil reference.

Table S4 Linear combination results CO oxidation.

Position	**Pd foil contribution**	**Error**	**PdO contribution**	**error**
0	0.836897	0.0112	0.163103	0.0112
1	0.837192	0.009618	0.162808	0.009618
2	0.832641	0.009252	0.167359	0.009252
3	0.840884	0.010481	0.159116	0.010481
4	0.845242	0.011755	0.154758	0.011755
5	0.842323	0.01084	0.157677	0.01084
6	0.826897	0.013228	0.173103	0.013228
7	0.717437	0.013152	0.282563	0.013152
8	0.652439	0.011039	0.347561	0.011039
9	0.615944	0.012819	0.384056	0.012819
10	0.584932	0.012997	0.415068	0.012997
11	0.533537	0.013547	0.466463	0.013547
12	0.527091	0.015707	0.472909	0.015707

Table S5 Linear combination results CO oxidation with H_2.

Position	Pd foil contribution	Error	PdO contribution	error
0	0.861833	0.010727	0.138167	0.010727
1	0.700693	0.011664	0.299307	0.011664
2	0.662059	0.010674	0.337941	0.010674
3	0.670556	0.013166	0.329444	0.013166
4	0.660007	0.012729	0.339993	0.012729
5	0.654013	0.012367	0.345987	0.012367
6	0.657703	0.012803	0.342297	0.012803
7	0.635175	0.012059	0.364825	0.012059
8	0.607668	0.012735	0.392332	0.012735
9	0.578569	0.012867	0.421431	0.012867
10	0.559521	0.013739	0.440479	0.013739
11	0.536825	0.014619	0.463175	0.014619
12	0.520124	0.015764	0.479876	0.015764

TAP

Knudsen Diffusion:

In a TAP experiment the use of a small number of molecules combined with the constant evacuation of the micro-reactor leads to the elimination of any gas-gas interactions. Therefore convectional transport is eliminated and the transport of gaseous molecules in the micro-reactor occurs solely by Knudsen diffusion, the diffusivity of which is defined in Equation S1.

$$D = \frac{\varepsilon}{\tau_{tor}} \frac{d_i}{3} \sqrt{\frac{8RT}{\pi M_w}}; \text{ where } d_i = \frac{4\varepsilon}{3(1-\varepsilon)} r_p$$

Equation S1

The diffusional flow rate through the reactor cross section is proportional to the cross sectional area of the reactor, the effective diffusivity and the gas concentration gradient, as shown in Equation S2.

$$F = -A_r D \frac{\partial C_g}{\partial x}$$

Equation S2

The rates of chemical transformation can be measured in the diffusion + reaction experiment based on information about diffusion transport. In a diffusion-reaction case: this entails the inclusion of an inert gas with the reaction mix. The use of the inert molecules allows characterization of the Knudsen diffusion transport for the specific micro-reactor packing, including the catalyst. As shown in Equation S2, the Knudsen diffusivity for the same packing at the same temperature is proportional to the inversed square root of molecular weight. Using this relationship, the diffusivity (or residence time) obtained for the inert molecules can be renormalized to characterize other reactant/product molecules.

In a pulse-response TAP experiment, the rates of chemical transformation or gas concentrations are not measured directly. In the observed responses (i.e. exit flow time dependencies) reaction rates are coupled with Knudsen transport. Thus, in order to obtain the rate constants of chemical

transformation, a theoretical model for Knudsen diffusion combined with reaction rate needs to be applied for the analysis of the data gathered in a TAP experiment.

Moment Based Analysis:

In TAP data analysis, the intensity (area) and the shape of the experimental response curves are compared with the theoretical model in order to extract kinetic information. A TAP pulse response defines the exit flows of specific molecules from the micro-reactor as a function of time. A TAP response starts from zero (the reactor is initially evacuated) passes through a maximum and reaches zero again (all molecules are evacuated in the end). Both intensity and shape of such curve can be analysed using moments, which are integrals of the observed TAP pulse responses weighted with a different power of time as demonstrated in Equation S3.

$$M_n = \int_0^{+\infty} t^n F(t) dt$$

Equation S3

The 0th moment (M_0) is the integral of observed exit flow and has the units of moles. It is used to determine the total number of molecules leaving the reactor after a single pulse (used to calculate conversion).

The 1st moment (M_1) has the unit of mole*s and is used to determine the residence time of a species (see Equation S5 below).

The 2nd moment (M_2) has the units of mole*s^2 and determines the dispersion of residence time that can be related to the characteristic time of observed kinetic processes e.g. desorption or porous diffusion.

For an inert gas the diffusional model can be solved using different methods (e.g. the method of separation of variables[3] or Laplace transformation[4]). Since no reaction is assumed, the area under the responses merely reproduces the pulse intensity. The following form of the area normalized solution for observed exit flow can be used to generate the diffusional response, as shown in Equation S4[5]:

 , where $\tau_{res}=\frac{\varepsilon L_r^2}{2D}$

Equation S4

According to Equation S4, the diffusional response is determined by only one parameter, which can be used for fitting experimental curves. This parameter can be determined by calculating the first moment of the response, M_1, which gives the residence time in the reactor, as defined in Equation S5:

$$\frac{M_1}{M_0}=\frac{\varepsilon L_r^2}{2D}=\tau_{res}$$

Equation S5

The purely diffusional residence time (first moment) depends on temperature and molecular weight of the probe molecule according to the Knudsen diffusion theory as is defined by Equation S6[5]:

Equation S6

The thin zone TAP reactor (TZTR) configuration, where the catalyst zone is made very narrow with respect to the entire length of the micro-reactor thereby allowing a near uniform catalyst composition[6], was adopted for the experiments. The specifics of the model are reported elsewhere[7], as is the methodology for the derivation of the basic kinetic coefficients, and how these are used to determine the adsorption rate constant, k_a.[8,9]

Notation

A_r	cross sectional area of the reactor (m^2)
C_g	gas concentration (mol m^{-3})
d_i	diameter of channels between particles
D	Knudsen diffusivity (cm^2 s^{-1})
F	area-normalized exit flow (s^{-1})
L_r	length of the reactor (m)
M_n	moment of n^{th} order (mole s^n)
M_w	molecular weight
R	universal gas constant
t	time coordinate (s)
T	temperature (K)
x	space coordinate (m)
τ_{tor}	toruosity
τ_{res}	mean residence time (s)
ε	bed voidage

Supporting TAP Results

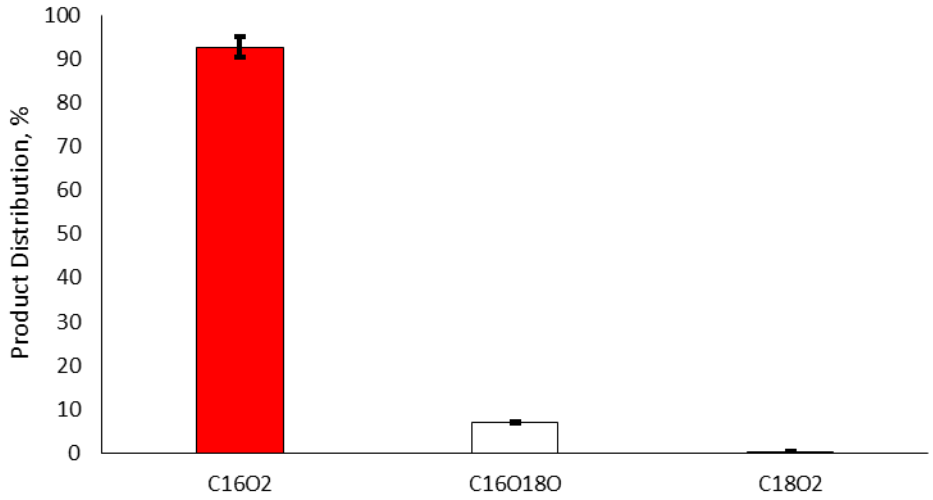

Figure S7 Distribution of differently labelled carbon dioxide molecules ($C^{16}O_2$ (red), $C^{16}O^{18}O$ (white) and $C^{18}O_2$ (black)) formed upon simultaneous pulsing of $^{18}O_2$:Ne =1:1 and CO_2:Ar =1:1 mixtures at 200°C over Pd/Al_2O_3 pre-treated in $^{16}O_2$.

References

[1] Dai, C.; Li, Y.; Ning, C.; Zhang, W.; Wang, X.; Zhang, C. The influence of alumina phases on the performance of Pd/Al2O3 catalyst in selective hydrogenation of benzonitrile to benzylamine, *Appl. Catal. A* **2017**, *545*, 97-103.

[2] Huang, S.; Zhang, C.; He, H. Effect of pretreatment on Pd/Al2O3 catalyst for catalytic oxidation of o-xylene at low temperature, *J. Envrion. Sci.* **2013**, *25*, 1206-1212.

[3] Yablonsky, G.S.; Olea, M.; Marin, G.B. Temporal analysis of products: basic principles, applications, and theory *J. Catal*. **2003**, *216*, 120-134.

[4] Constales, D.; Shekhtman, S.O.; Marin, G.B.; Yablonsky, G.S.; Gleaves J.T. Multi-zone TAP-reactors theory and application IV. Ideal and non-ideal boundary conditions *Chem. Eng. Sci.* **2006**, *61*, 1878-1891.

[5] Gleaves, J.T.; Yablonskii, G.S.; Phanawadee, P.; Schuurman, Y. TAP-2: An interrogative kinetics approach *Appl. Catal*. *A* **1997**, *160,* 55-88.

[6] Shekhtman, S.O.; Yablonsky, G.S.; Chen, S.; Gleaves, J.T. Thin-zone TAP-reactor - theory and application, *Chem. Eng. Sci.*, **1999**, *54*, 4371-4378.

[7] Shekhtman, S.O.; Yablonsky, G.S.; Gleaves, J.T.; Fushimi R. Thin-zone TAP reactor as a basis of "state-by-state transient screening", *Chem. Eng. Sci.* **2004**, *59*, 5493-5500.

[8] Shekhtman, S.O.; Yablonsky, G.S.; Gleaves, J.T.; Fushimi R. "State defining" experiment in chemical kinetics—primary characterization of catalyst activity in a TAP experiment, *Chem. Eng. Sci.* **2003**, *58*, 4843-4859.

[9] Shekhtman, S.O.; Maguire, N.; Goguet, A.; Burch, R.; Hardacre, C. Three primary kinetic characteristics observed in a pulse-response TAP experiment, *Catal. Today* **2007**, *121*, 255-260.